Available online at www.sciencedirect.com
SCIENCE DIRECT®
Journal of Nuclear Materials 344 (2005) 104–108
journal of nuclear materials
www.elsevier.com/locate/jnucmat

Structural investigation on lead fluoride–lithium fluoride at various compositions and temperatures

S. Watanabe [a,*], H. Matsuura [a], H. Akatsuka [a], Y. Okamoto [b], P.A. Madden [c]

[a] Research Laboratory for Nuclear Reactors, Tokyo Institute of Technology, O-okayama, Meguro-ku, Tokyo 152-8550, Japan
[b] Department of Materials Science, Japan Atomic Energy Research Institute, Tokai-mura, Naka-gun, Ibaraki 319-1195, Japan
[c] Physical and Theoretical Chemistry Laboratory, Oxford University, South Parks Road, Oxford OX1 3QZ, UK

Abstract

Local structure around lead ion of molten PbF_2–LiF system at various compositions ($x_{PbF_2} = 0.2$, 0.4, 0.6, 0.8 and 1.0) were investigated by extended X-ray absorption fine structure (EXAFS) analysis, and composition dependence of the local structure was revealed. Coordination number and inter-ionic distance between 1st neighboring Pb^{2+}–F^- show similar to each other except at eutectic composition. In addition, structural change observed in EXAFS signals of pure PbF_2 is reproduced by molecular dynamics simulation with polarization ion model.

1. Introduction

Molten PbF_2–LiF is one of candidate materials for fusion blanket, and we have evaluated various properties of this system, e.g. eutectic composition (PbF_2: 60 mol%, 850 K) [1], suitable metal for the construction materials [2], chemical form of tritium released from the molten salt when thermal neutrons were irradiated [3], tritium inventory simulated by measuring solubility of hydrogen fluoride [4] and local structure around lead ion of pure PbF_2 and eutectic PbF_2–LiF at various temperatures [5].

In this study, we have obtained the new EXAFS results of molten $x$$PbF_2$–$(1-x)$LiF systems ($x_{PbF_2} = 0.2$, 0.4, 0.6, 0.8, 1.0), and discuss the composition dependence on the local structure around lead ion. These results will be helpful to decide the practical composition for molten salt fusion blanket since the local structure of molten salt affects considerably on the physico-chemical properties of the molten salt such as electric and thermal conductivity, viscosity and compressibility, etc. Local structural information of the molten salt can be linked with such properties by computer simulations. In order to reproduce the local structure of the molten salts by computer simulation, well-defined inter-ionic potential that can reproduce properties both in solid and liquid phases must be chosen and developed. However, there are still quite a few potential settings which can reproduce the experimental data due to super ionic conductance behavior of solid PbF_2 or strong polarizability of Pb^{2+} ion.

In previous our paper [5], we have reported structural change in solid PbF_2 at high temperature caused by superionic conductance phase transition along with the local structures of liquid phases. The interpretation of the structural change is important not only for designing the superionic conductors but also for optimizing the inter-ionic potential between Pb^{2+} and F^-. Therefore, in the present study, we tried to reproduce the structural change of solid PbF_2 from room temperature until high

* Corresponding author. Tel./fax: +81 3 5734 3057.
E-mail address: souwata@nr.titech.ac.jp (S. Watanabe).

0022-3115/$ - see front matter © 2005 Elsevier B.V. All rights reserved.
doi:10.1016/j.jnucmat.2005.04.025

temperature phases (i.e. α phase → β phase → superionic conductance phase) by molecular dynamics simulation as well.

2. Experiment

PbF_2 (Soekawa Chemical Co., 5 N, m.p. = 1128 K) and superpure quality LiF (Wako, m.p. = 1121 K) were melted in a glassy carbon crucible at approximately 1173 K, and then cooled down to room temperature in dried Ar atmosphere environment. Samples are subdivided into micrometric sized particles and mixed with BN matrix powder homogeneously in an agate mortar placed in the glove box filled with dried Ar gas. These powders were pressed into pellets with approximately 1 mm thickness and 13 mm diameter. These pellets were installed into an electric furnace located between two ionization chambers. The electric furnace heated the sample up to 50 K above the melting point of the each composition. Melting points of xPbF$_2$–$(1-x)$LiF are approximately 1050, 1000, 850, 950 and 1090 K for x = 0.2, 0.4, 0.6, 0.8 and 1.0, respectively [1]. Sample environment was He gas throughout the EXAFS experiments.

Transmission XAFS measurements were performed using BL10B beamline at Photon Factory (PF) in the High Energy Accelerator Organization, Tsukuba, Japan (2.5 GeV, 200–400 mA) with energetic range of X-ray (12.54–14.14 keV) for Pb–L_{III} X-ray absorption edge (13.04 keV). X-ray absorption spectra were obtained by stepped scan measurement for 1 s at each energy. The synchrotron radiation was monochromatized by channel-cut Si(3 1 1) crystal. The number of incident and transmitted photons were counted by ionization chambers with Ar + N_2 (1:1) and Ar, respectively.

XAFS data analysis was carried out using WinXAS Ver. 2.3 [6] as following procedure. XAFS oscillation $\chi(k)$ was obtained by removing smooth atomic background from a normalized absorption spectrum by assuming the combination of 2nd degree polynomials. The structural function FT $|\chi(k)\cdot k^3|$ was obtained by Fourier transforming the k^3 weighted $\chi(k)$ function multiplied by a Bessel window function with the range of $2.5 < k < 10.0$ Å^{-1}. Curve fitting analysis was done by nonlinear least square fits of Eq. (1) on predominant Pb^{2+}–F^- correlation peak in R-space,

$$\chi(k) = S_0^2 \frac{N_{\mathrm{PbF}} F(k)}{k R_{\mathrm{PbF}}^2} \exp\left(-2\sigma^2 k^2 + \frac{2}{3} C_4 k^4\right) \times \sin\left(2kR_{\mathrm{LnF}} + \delta(k) - \frac{4}{3} C_3 k^3\right), \quad (1)$$

where S_0^2 is the probability of single electron excitation, N_{PbF} the coordination number of F^- at distance R_{PbF} from Pb^{2+}, σ^2 Debye Waller factor which reflects thermal and structural disorder. C_3 and C_4 are the 3rd and 4th cumulants, respectively, which represent anharmonic oscillation effects at high temperature. $F(k)$ and $\delta(k)$ are the backscattering amplitude and phase shift of photoelectron, respectively, and they are derived from FEFF8.0 code [7].

Molecular dynamics simulations on PbF_2 at various temperatures have been performed by using polarizable ion model developed by Castiglione and Madden et al. [8]. We utilized NVT ensemble for equilibration, and exploited the same inter-ionic potential as [8]. After equilibration, the coordination data in every 100 steps were introduced to FEFF8.0 code in order to calculate EXAFS oscillation $\chi(k)$ as thermally averaging structure [9].

3. Results and discussion

EXAFS oscillations $\chi(k)\cdot k^3$ and Fourier transformed radial structural functions $|\mathrm{FT}(\chi(k)\cdot k^3)|$ of molten xLiF–$(1-x)$PbF$_2$ are shown in Figs. 1 and 2, respectively. Since there are differences of sample temperatures, intensity of oscillations or predominant peaks cannot be compared directly. However, difference of phases in Fig. 1 and peak positions in Fig. 2 show that the local structure of these molten salts seems to depend on the composition.

Structural parameters obtained by curve fitting analysis are listed in Table 1. Single electron excitation probability S_0^2 is evaluated to be 0.389 by the curve fitting of β-PbF_2 at 573 K, which takes symmetric cubic structure

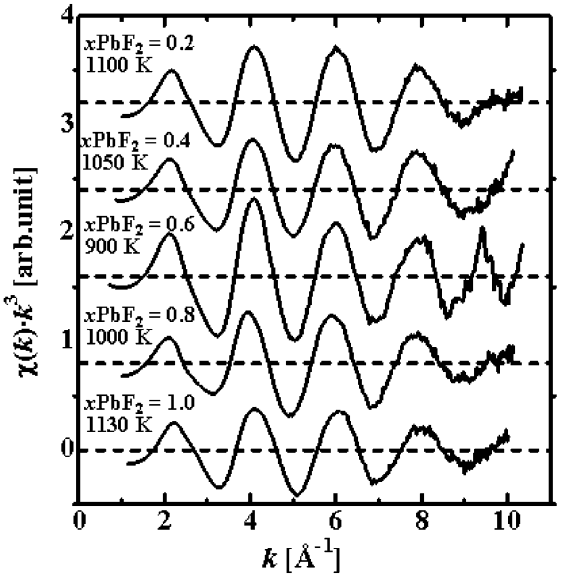

Fig. 1. EXAFS oscillations $\chi(k)\cdot k^3$ of molten xPbF$_2$–$(1-x)$LiF.

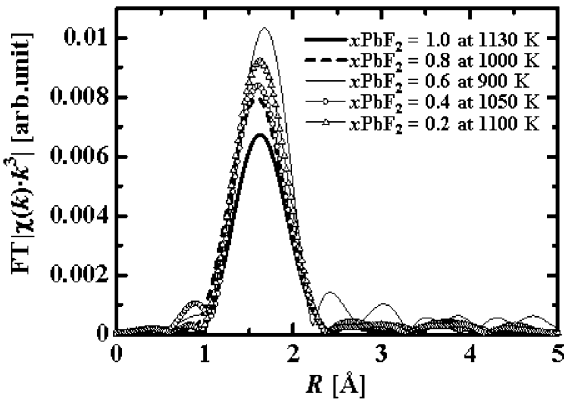

Fig. 2. Radial structural functions $|\mathrm{FT}(\chi(k)\cdot k^3)|$ of molten $x\mathrm{PbF_2}$–$(1-x)$LiF.

[10], usually used as a standard sample. Although $S_0^2 = 0.8$–1.0 is general for EXAFS analysis, this value might be reasonable, because double-electron excitation and triple-electron excitation, which reduce the S_0^2 value, are reported at about 180 eV and 410 eV above the L_{III} threshold energy [11], respectively.

Coordination number and inter-ionic distances of these molten salts show similar to each other except those at eutectic composition, i.e. $N_{\mathrm{PbF}} = 5.39$ and $R_{\mathrm{PbF}} = 2.39$ Å for eutectic composition and $N_{\mathrm{PbF}} = 3.76$–4.58, $R_{\mathrm{PbF}} = 2.35$–2.36 Å for others. These values are reasonable with respect of the sum of ionic radii since ionic radius of Pb^{2+} becomes larger as increasing the coordination number (1.12 Å for 4-coordinated, 1.33 Å for 6-coordinated and 1.43 Å for 8-coordinated) [12].

N_{PbF} obtained in this study finely agree with those reported in [5], however R_{PbF} show slightly larger values than those in [5]. These differences might be caused by the difference of the k range used in Fourier transformation. We chose $2.5 < k < 7.5$ Å^{-1} for Fourier transformation in order to avoid multi-electron excitation effect and S_0^2 value was used as a fitting parameter in previous study [5], while multi-electron excitation effects is included in S_0^2 and wider k region is used in this study. Therefore Pb^{2+}–F^- correlation peak in radial structural function become sharper than previous one, and more reliable R_{PbF} values can be obtained.

Although coordination number and inter-ionic distance are evaluated as the average value of various clusters PbF_n existing in the molten salts, 4-coordinated tetrahedral PbF_4^{2-} geometry seems to be predominant both in molten pure PbF_2 and in LiF–PbF_2 mixtures, except only at around eutectic composition. 6-coordinated hexahedral PbF_6^{4-} geometry might be the most stable in eutectic composition. These results suggest that additive amount of Li^+ hardly affects on the local structure around Pb^{2+} except for the eutectic composition. This unique structural property at eutectic composition may be caused by thermodynamical specific characteristics of the molten salt, although lower temperature of the molten salt is also considered to be one of the reasons of higher coordination number and inter-ionic distance.

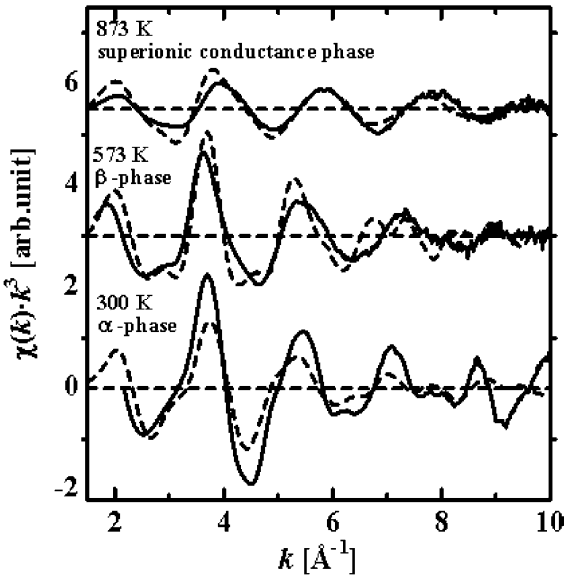

Fig. 3. EXAFS oscillations $\chi(k)\cdot k^3$ obtained by MD and experiments at 300, 573 and 873 K. Solid line and dashed line correspond to experimental and calculated spectrum, respectively.

Table 1
Structural parameters obtained by curve fitting analysis

$x\mathrm{PbF_2}$	T (K)	N_{PbF}	R_{PbF}	σ^2 (10^{-2} Å^2)	C_3 (10^{-3} Å^3)	C_4 (10^{-4} Å^4)	Residual
1.0	1130	3.76	2.36	3.17	3.66	6.93	8.28
0.8	1000	3.90	2.35	2.62	3.40	4.60	9.96
0.6	900	5.39	2.39	2.71	3.71	4.53	8.18
0.4	1050	4.35	2.35	2.88	3.26	5.44	7.98
0.2	1100	4.58	2.36	2.80	3.67	5.00	9.35

Residual is defined by residual $[\%] = 100 \cdot \sum_{i=1}|\chi_{\mathrm{exp}}(i) - \chi_{\mathrm{cal}}(i)|/\sum_i|\chi_{\mathrm{exp}}(i)|$, and characters exp and cal corresponds to experimental and calculation, respectively.

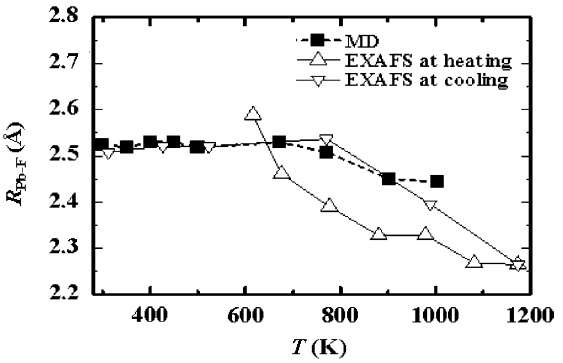

Fig. 4. Temperature dependence of inter-ionic distance between Pb^{2+}–F^- derived from EXAFS and MD.

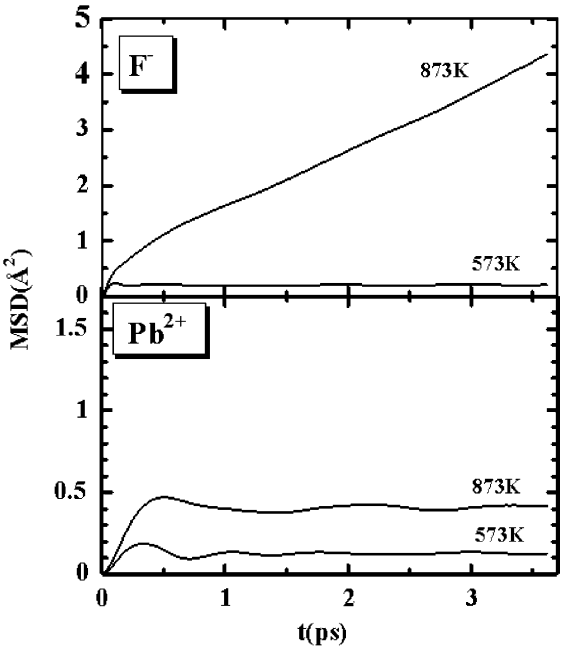

Fig. 5. Mean square displacement of Pb^{2+} and F^- at 573 K and 873 K.

Therefore, eutectic LiF–PbF_2 should be more investigated especially at higher temperature ranges.

EXAFS oscillations $\chi(k)\cdot k^3$ of pure PbF_2 calculated by MD simulation along with experimental data at 300, 573 and 873 K are shown in Fig. 3. Spectra at 300, 573 and 873 K correspond to those at α, β and superionic conductance phase, respectively. Still there have slight discrepancy in amplitude, but oscillation phases are almost reproduced. The temperature dependences on inter-ionic distances derived from MD and EXAFS experiments are shown in Fig. 4. The mean square displacement of Pb^{2+} and F^- both at 573 K and 873 K are shown in Fig. 5. Between 573 and 873 K, F^- ions are drastically transferable, inter-ionic distance R_{PbF} decreases in superionic conduction phase.

The inter-ionic potentials suggested in [8] are considered to be almost optimized, because the tendency of varying inter-ionic distance in solid state is perfectly reproduced. However, in this study, EXAFS signals and structural parameters of molten PbF_2 are not successfully reproduced by the MD simulation due to lack of density information at liquid state. For quantitative discussion in detail, further experiments and MD simulation on LiF–PbF_2 system would be required.

4. Conclusion

Composition dependence on local structure around lead ion in molten $x$$PbF_2$–$(1-x)$LiF systems are revealed to that 6-coordinated hexahedral and 4-coordinated tetrahedral geometry are predominantly existing in eutectic composition and other compositions, respectively. In addition, Pb^{2+}–F^- inter-ionic potential is optimized to reproduce the temperature dependence of solid PbF_2 EXAFS signals by MD simulations. Other experimental data, such as density of molten salts and local structure of molten LiF, will be helpful for performing MD simulation of molten PbF_2 and $x$$PbF_2$–$(1-x)$LiF. In order to evaluate more practical applications of molten $x$$PbF_2$–$(1-x)$LiF systems for fusion blanket, relations between various physico-chemical properties and local structures obtained by EXAFS and another techniques conjunction with MD simulations must be explored.

Acknowledgments

We are grateful to Drs Akihiko Kajinami (Kobe University) and Mitsuo Matsuzaki (Tokyo Institute of Technology) for assistance with EXAFS experiments. EXAFS experiments have been performed under the proposal No. 2003G084. The work was supported by JSPS No. 99GC0006, and COE21 program for SW.

References

[1] N. Saito, K. Kawamura, H. Tanaka, R. Takagi, Denki Kagaku (Electrochemistry) 54 (10) (1986) 864.
[2] K. Kawamura, H. Tanaka, N. Saito, R. Takagi, Denki Kagaku (Electrochemistry) 55 (9) (1987) 684.
[3] K. Kawamura, G.G. Li, R. Takagi, N. Horiuchi, Denki Kagaku (Electrochemistry) 59 (5) (1991) 438.
[4] M. Ablanov, H. Matsuura, R. Takagi, J. Nucl. Mater. 258–263 (1998) 500.

[5] S. Watanabe, R. Toyoyoshi, T. Sakamoto, Y. Okamoto, Y. Iwadate, H. Akatsuka, H. Matsuura, Phys. Scr. T 115 (2005) 297.
[6] T. Ressler, J. Phys. IV 7 (1997) C2.
[7] S.I. Zabinsky, J.J. Rehr, A. Aukudinov, R.C. Albers, M.J. Eller, Phys. Rev. B 52 (1995) 2995.
[8] M.J. Castiglione, P.A. Madden, J. Phys.: Condens. Matter. 13 (2001) 1.
[9] Y. Okamoto, T. Yaita, K. Minato, J. Non-Cryst. Solids 333 (2004) 182.
[10] R.W.G. Wyckoff, 2nd Ed., Crystal Structures, vol. 2, Interscience, 1964.
[11] A.D. Cicco, A. Filipponi, Phys. Rev. B 49 (18) (1994) 49.
[12] R.D. Shannon, Acta Crystallogr. A32 (1976) 751.